CMS Internal Note

The content of this note is intended for CMS internal use and distribution only

Afterpulses in HF Photomultiplier Tubes and Consequences

Nural Akchurin[1], Oleksiy Atramentov[2], Heejong Kim[1]

[1] *Texas Tech University, Department of Physics, Lubbock, TX, USA*

[2] *Iowa State University, Department of Physics, Ames, IA, USA*

Abstract

Upon observation of spurious pulses that arrived several hundreds of nanoseconds after the main PMT pulse, we performed a series of measurements to quantify this effect. The characteristic property of these afterpulses is that they come hundreds of nanoseconds later than the main pulse, their rate depends on the magnitude of the main pulse, and the charge of the afterpulse is approximately constant regardless of the main pulse amplitude. If ascribed to gas impurities in the PMT vacuum, the time distribution of these afterpulses depends on the mass of gas impurity as $\sqrt{m}$ where m is the mass of the singly charged feed-back ion. We show that the lab measurements are consistent with the beam tests in 2004 using QIE front-end electronics. We also estimate the contribution of the afterpulses to the missing transverse energy.

1 Introduction

The Hamamatsu R7525 photomultiplier tube (PMT) was chosen for the forward calorimeter (HF) of the Compact Muon Solenoid (CMS) experiment because it had the appropriate gain (10^4 to 10^5) with adequate quantum efficiency ($\sim 20\%$) and photocathode window transparency ($> 90\%$). Each of these PMTs was tested for gain, dark current, and other properties [1]. It was found, however, that there were noticable afterpulses in a number of PMTs early 2004.

When the concentration of gas impurities (H_2, He, CH_4, N_2, *etc.*) in the PMT volume reach high levels ($\geq$ 1 ppm), they are likely to be produced at the first dynode. Consequently these ions slowly drift and accelerate towards the photocathode. Upon impact with the photocathode, they release electrons which in turn form these afterpulses [2, 3, 4, 5, 6, 7]. The time it takes for these ions to reach the photocathode can be simply estimated as $\sqrt{2mx/(qE)}$ where m is the mass of the ionized molecule, x is the distance from the point of ionization to the photocathode (or the distance between the first dynode and the photocathode), q is the ion charge (assumed to be $+e$), and E is the electric field. Therefore, the H_2^+ ion would take ~ 60 times longer compared to an electron to traverse the same distance. The helium ion would be slower by a factor of ~ 90.

We briefly describe the experimental setup in Section 2. In Section 3, the time spectra and the afterpulse rates are discussed under different test conditions. In an attempt to investigate the connection between the afterpulse rates and production batches, we tested one PMT from each of nine production batches. We found that the behavior of the PMTs could be categorized in three groups. We summarize these results, along with the major results from the 2004 beam tests at CERN, in Section 4. In Section 5, we draw attention to the consequences of these types of afterpulses to the performance of the CMS forward calorimeter. We summarize our conclusions in Section 6.

2 Experimental Setup

The experimental setup is depicted in Figure 1. A blue LED serves as the pulsed light source and is driven by a 25 ns-wide square pulse. The CAEN N472 unit supplies the nominal high voltage value of -1300 V ($g \approx 10^5$). For some measurments, the PMT signal was amplified by a fast amplifier with a gain factor of ~ 10. An amplification factor of 100 was obtained by cascading the signals when working with small initial pulses as needed. The amplified PMT output was fanned out and digitized. Both the main pulse and the afterpulse were fed into two ADCs with different gates in time. In addition, the timing of the afterpulses was recorded by a TDC in order to study the timing distribution of these afterpulses.

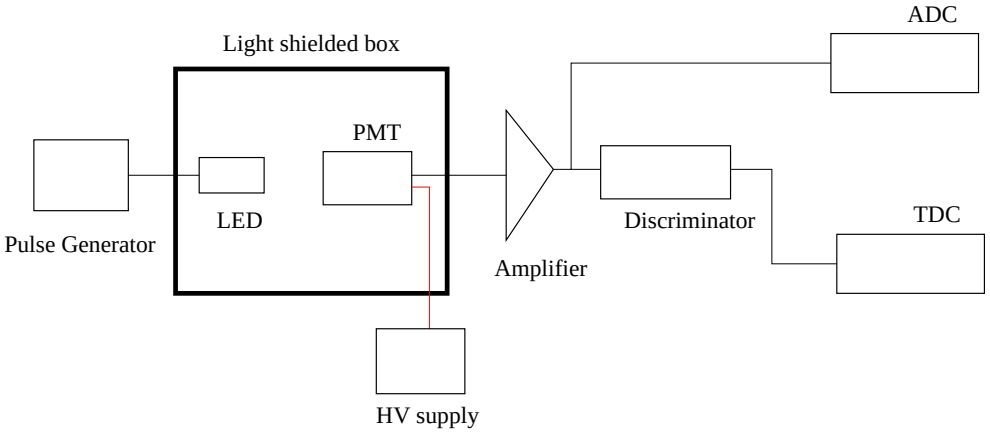

Figure 1: The schematic diagram of the bench setup is shown above. We used standard NIM and CAMAC electronics for all measurements.

3 Results

3.1 Tests with a Single PMT

We define the afterpulse rate as follows.

$$\text{Afterpulse rate}\,(\%) = \frac{\text{Number of events with afterpulse}}{\text{Total number of events}} \times 100. \quad (1)$$

We first randomly selected a single PMT (SN:1522) to determine the correlations between the afterpulse, the main pulse amplitude, and LED driver frequency. The timing and rate of the afterpulses were measured as a function of these parameters. The PMT amplitude was set to 300 mV regardless of the amplication factors by adjusting the LED bias voltage. In nominal HF operation, 30 mV output pulse corresponds approximately to ≥ 1 TeV. Therefore, we strived to cover a wide range in bench tests from $\sim$1 GeV to $\sim$10 TeV. The lower end ($\sim$1 GeV) was set by the least count of available ADCs (250 fC/count divided by 100).

Figure 2 shows the timing distribution of the afterpulses in nanoseconds for the first tested PMT . In the case of multiple afterpulses in an event, the TDC recorded the first one only because we were limited by single-hit TDCs. For this particular PMT, the afterpulses typically took place $\sim$350 ns after the main pulse.

Figure 3 shows the afterpulse rate as a function of the discriminator threshold. The threshold level was varied from 30 mV to 110 mV, and the sudden drop of the afterpulse rate in 30 to 50 mV range indicates that most of afterpulses have constant pulse heights. This was also confirmed when the afterpulse charge was directly measured, which will be discussed later in this section.

Figure 4 indicates that the afterpulse rate is independent of the LED flash frequency. Although the data acquisition system suffered from large dead-time in $> 10^3$ Hz, this didn't affect the quality of the measurement.

The gain dependence of the afterpulse rate is shown in Figure 5. The main pulse heights of the PMT (after amplification) were kept near 300 mV when the high voltage was varied. In other words, the LED driver amplitude was tuned such that at any HV bias the PMT output would be fixed at 300 mV. The afterpulse rate increased linearly with PMT gain and was negligible when the high voltage was less than -1100 V. Note that in this measurment the number of photons on the photocathode decreases with increasing high voltage: the parameter that is kept constant is the output amplitude of the PMT.

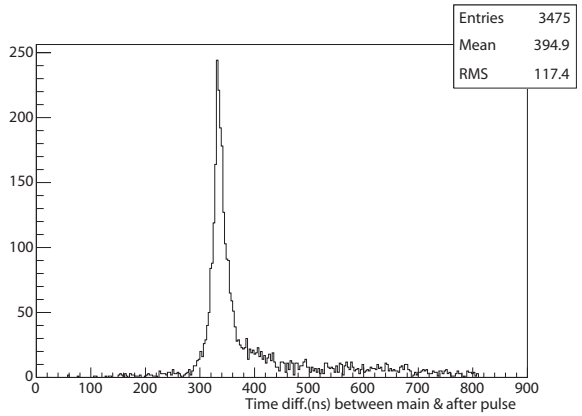

Figure 2: The timing distribution of the afterpulse for the first tested PMT shows that majority of the afterpulses arrive at $\sim$350 ns after the main pulse.

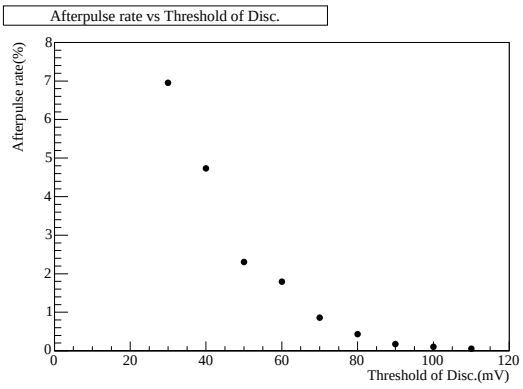

Figure 3: The abrupt fall of afterpulse rate (30 to 50 mV) as a function of the discriminator threshold illustrates that the afterpulses are nearly constant in amplitude.

The total afterpulse charge was integrated by an ADC, and Figure 6 shows the total afterpulse as a function of the main pulse charge. The afterpulse essentially remains constant for a wide range of main pulse.

Irrespective of how the main pulse charge changes, once the ions are made they will propagate towards the photocathode and release electrons from the photocathode essentially in the same manner at all times. If we consider a total ionization cross section of 2×10^{-16} cm^2 for 300 eV electrons (typically between 0.5 to 2.4 $\times 10^{-16}$ cm^2 for the gases in questions here), we expect to ionize atoms/molecules 0.054% of the time near the first dynode (1 mm) at a partial pressure of 10^{-6}. When these ions impact the photocathode, they release 5 to 10 electrons. Therefore, the amount of charge an afterpulse carries is approximately constant regardless of the ionization and recombination processes invloved in the PMT envelope. The rate at which these ions are generated, however, will depend on the main pulse charge. As the main pulse charge grows, the probability that a gas molecule is ionized increases linearly.

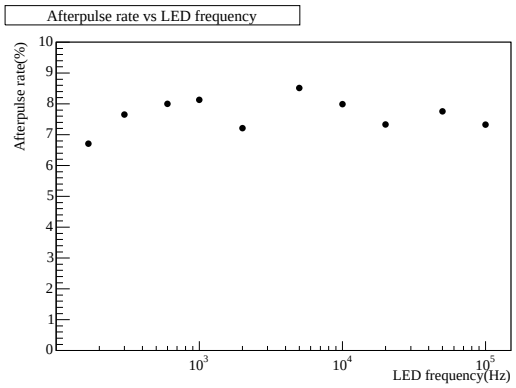

Figure 4: The afterpulse rate does not change with the frequency of the LED induced pulses in the range measured, from a few Hz to 10^5 Hz.

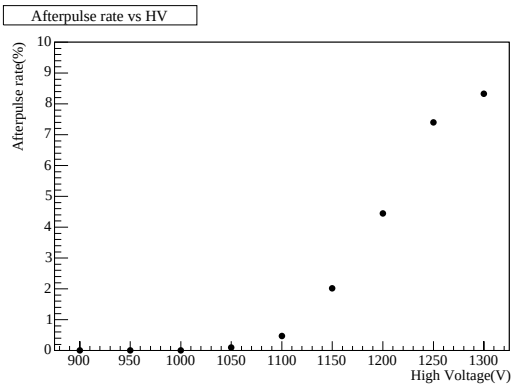

Figure 5: The afterpulse rate *vs* the applied HV shows nearly linear dependence (see text for details).

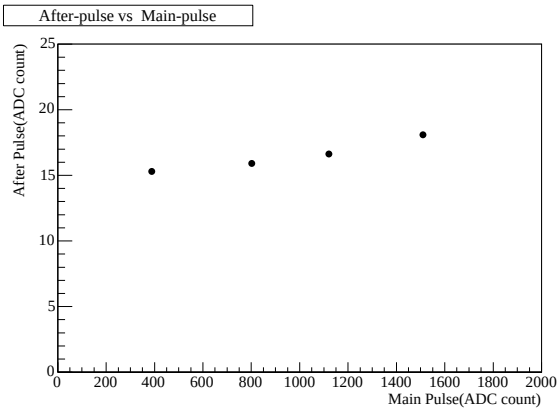

Figure 6: The afterpulse charge does not depend strongly on the charge carried by the main pulse. At –1300 V, the afterpulse is 375 fC when 10× amplification is taken into account (15 ADC × 0.25 pC /10 = 375 fC).

The main pulse signal of the PMT was reduced $\sim$ 10 times by making the input voltage to LED smaller. A 100 times amplified PMT signal was fed into the ADC to measure the effects of the smaller main pulse. The timing distribution of the afterpulse showed the same behavior as in Figure 2. The ADC values and rate of the afterpulse as a function of the main pulse are shown in Figures 7 and 8. The level of the ADC

for the afterpulse in Figure 7 was increased 10 times compared to Figure 6. These results confirm that the afterpulse had constant pulse height but that the rate was proportional to the main pulse height.

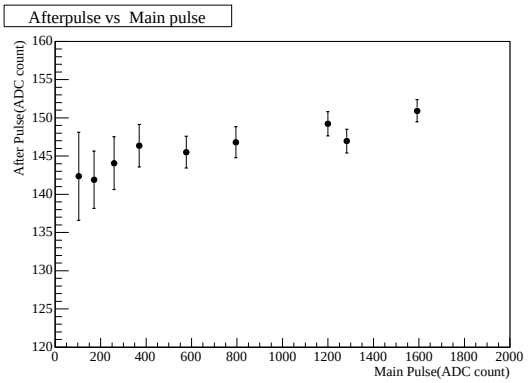

Figure 7: The afterpulse charge compared to the main pulse charge does not vary significantly, as indicated before (145 ADC counts × 250 fC / 100 = 362.5 fC).

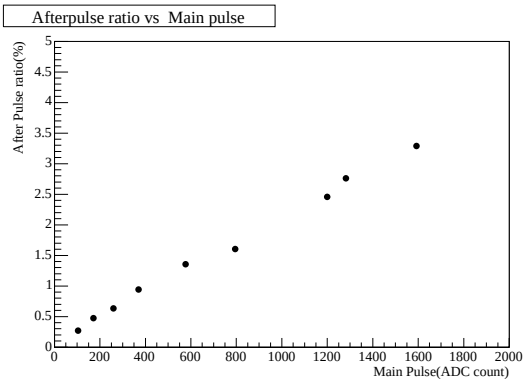

Figure 8: The afterpulse rate as a function of the main pulse charge linearly increases. One ADC count is effectively 2.5 fC which results in an afterpulse rate of 0.0004%/fC for this first sample PMT. This rate is to be contrasted with Type B in Figure 11.

3.2 Batch Tests

The results presented in the previous subsection were obtained from a single R7525 PMT. In order to see if the afterpulse rates were corralated with the production batches, we selected a single PMT from each batch (see Table 1).

Different degrees of afterpulses were found in all tested PMTs. The timing distributions of the afterpulses were not always the same as the sample PMT and could be categorized into three groups. The fourth column in Table 1 indicates that we chose to group the tested PMTs in three different groups based on their afterpulse timing distributions.

Table 1: Nine different R7525 PMTs were taken from nine different production batches. The serial number, the batch number, relative gain [1], and the type of afterpulse class it belongs to are tabulated for reference.

PMT S/N	Batch #	Relative gain(%)	Type
68	1	106	A
66	2	181	A
405	3	89	B
515	4	90	B
872	5	90	C
1078	6	149	C
1313	7	90	C
1817	8	175	C
2108	9	130	C

The timing distributions for these groups are shown in Figure 9. The type A PMT had only one peak

at ~ 330 ns while types B and C displayed three distinct peaks. In all three groups, ~ 330 ns peak was present while the early (~ 170 ns) and the late (~ 650 ns) peaks were visible only in types B and C (at –1350 V). The full-width half-maxima of these timing peaks are in the order of 20-40 ns. We ascribe these peaks to H_2^+, He^+ and possibly CH_4^+. The scaling of the peaks in the time distributions is not exact. We expect a ratio of 1.5 between the He^+ and H_2^+, and 2.0 between CH_4^+ and H_2^+. The timing distributions result in a ratio of 1.9 for He^+ and H_2^+, and 1.9 between CH_4^+ and H_2^+. It is not excluded that the heavier contamination can also be due to N_2^+, CO_2^+, and O_2^+ (see discussions in [4, 5, 8]).

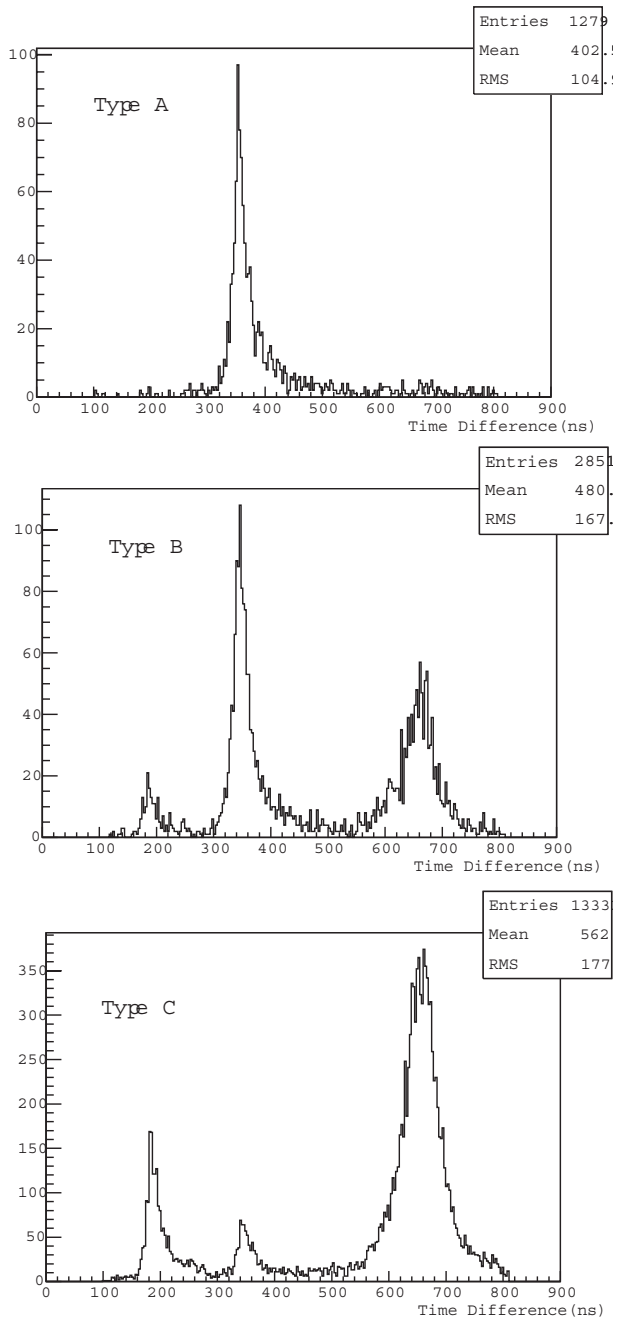

Figure 9: The typical afterpulse timing distributions from types A, B, and C exhibit characteristically different of ion feed-back time distributions. We group the PMTs into three types based on these distributions.

As previuously pointed out, the amount of charge carried by the afterpulse was essentially constant in

the sample PMT. This feature was found to be true in all of the PMTs. Figure 10 shows the pulse height of the afterpulse for these three groups. The gate positions for the ADC were adjusted to third peak for types B and C and for type A, the second peak was taken as the reference and was centered at ~ 330 ns.

Figure 11 shows that linear fits represent the afterpulse rate *vs* main pulse charge well. The slopes are 0.0006, 0.0017, and 0.0060%/fC for A, B and C groups, respectively. The rate for type C is generally 10 times higher than that of type A.

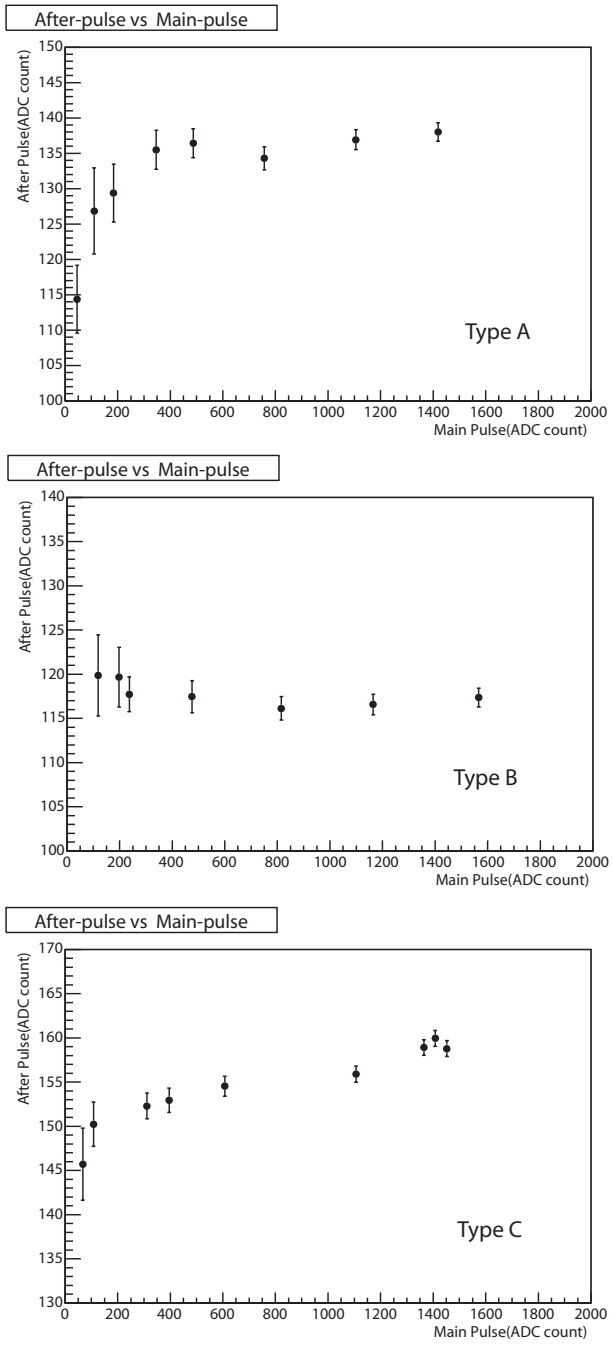

Figure 10: The charge (in ADC counts where 1 ADC count equals 2.5 fC) of the afterpulse as a function of the main pulse for three different PMTs from groups A, B, and C is essentially constant. Assuming 11 fC/GeV, each afterpulse fakes 25 to 35 GeV equivalent signal.

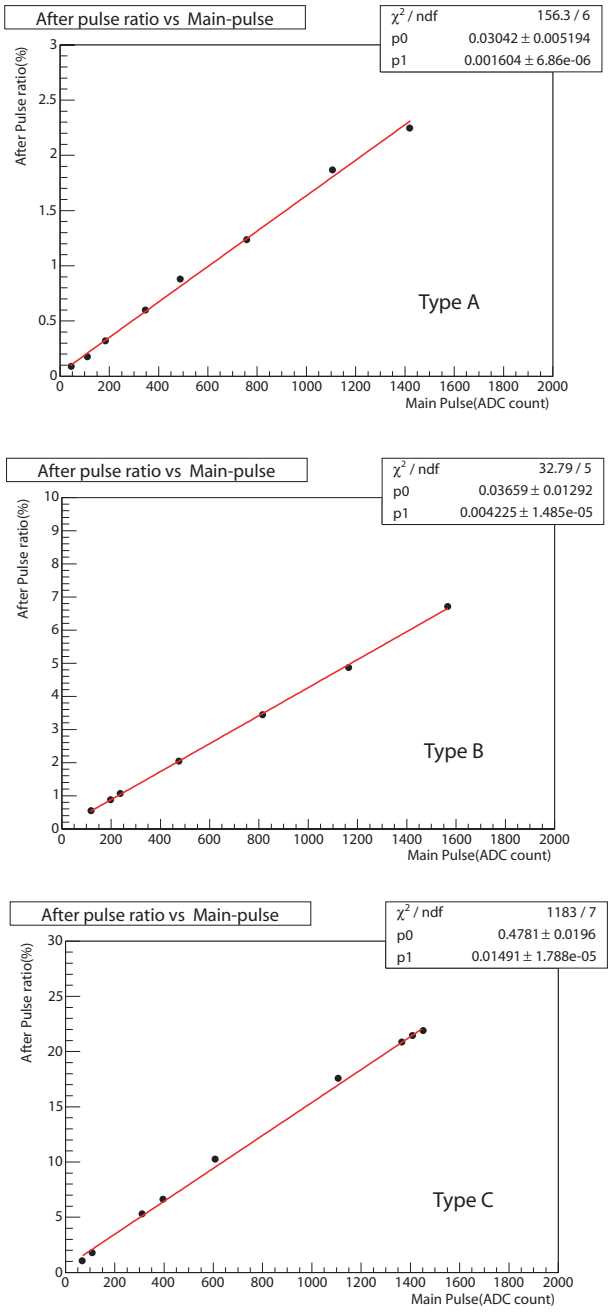

Figure 11: The afterpulse rate as a function of the main pulse for three different groups.The slopes are 0.0006, 0.0017, and 0.0060%/fC for A, B, and C groups, respectively. The rate for type C is generally 10 times higher than that of type A (1 ADC count effectively equals 2.5 fC).

We can estimate the energy equivalent of these afterpulses for the HF. Roughly ∼150 ADC counts equal 375 fC after taking into account a factor of 100 from the amplifier. Therefore, we expect the afterpulse energy to be ∼35 GeV (assuming 11 fC/GeV as explained in the following section).

4 Beam Tests

The HF pulses are digitized at 40 MHz with the QIE FE system. Therefore, every 25 ns, the output of the detector is digitized with a least count of 2.6 fC. These features enable us to measure the timing difference between the main pulse that is initiated by a high energy particle and the afterpulses that come from the contamination in the PMT envelope, the charges that are carried by the main and afterpulse, and the rate at which afterpulse occurs in a test beam. Figure 12 shows a typical event with a clear

afterpulse. The main pulse is due to a 100 GeV electron impinging the calorimeter (∼1100 fC) and the afterpulse of about half the charge ∼630 ns later. In this section we give detailed results for one PMT (EM tower 12). The average value for all the 24 PMTs for EM towers (long fibers) give afterpulse rates of 0.00044 ± 0.00027, 0.00091 ± 0.00184, and 0.00425 ± 0.00262 %/fC for the first, second, and third peaks, respectively.

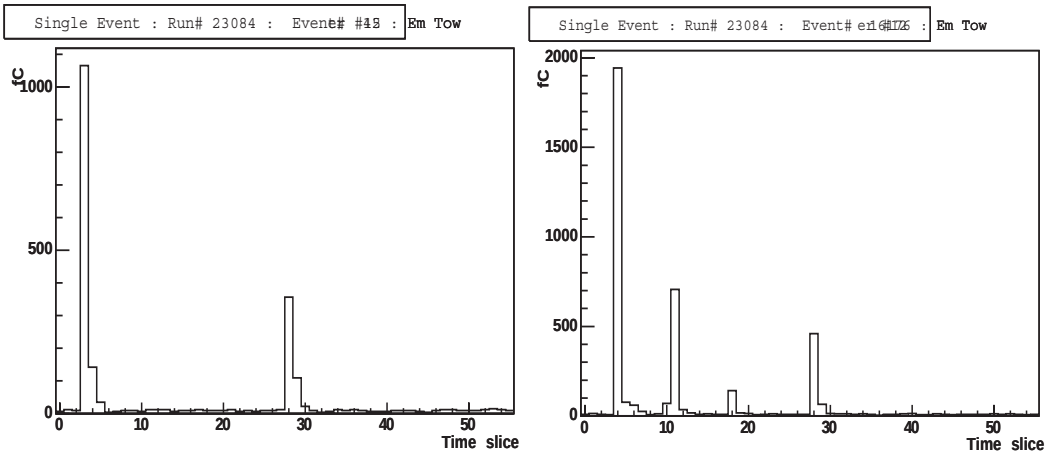

Figure 12: A clear single afterpulse for a 100-GeV electron impinging on the HF calorimeter comes ∼ 630 ns after the main pulse and is ∼40 GeV in energy scale (left). Note that one time slice is 25 ns wide. An unusual afterpulse event (right) shows all types of afterpulses in a single event for a 100-GeV electron at 175, 350, and 600 ns.

Timing of these afterpulses with respect to the main pulse depends on the electric field (E) between the photocathode and the first dynode as $1/\sqrt{E}$. Therefore, reducing the high voltage from –1350 V to –1150 V will induce a shift by +10%, as clearly seen in Figure 13.

Rate of afterpulse depends on the total main pulse charge as shown in Figure 14. Here, due to timing properties of the QIE, we can actually evaluate afterpulse rates –in particular time windows– individually. For the first, second, and third afterpulses, we calculate the 0.00084, 0.0011 and 0.0078 %/fC. Clearly, the third afterpulse dominates, at ∼ 0.01%/fC. The charge that is induced by these afterpulses is also measured individually as shown in Figure 15. On average, we can conclude that 100 GeV electron (1100 fC) would induce ∼10% of the time, 40 GeV equivalent energy, sometime within the next ∼ 700 ns after the main pulse. The probabilities are of course peaked at the times shown in Figure 13.

5 Consequences

We simulated the missing transverse energy distribution arising from these afterpulses using as inputs the pulse height and frequency distributions measured above, in addition to the calculated rate at which a mean number of 25 minimum bias events per crossing will populate the towers of HF. In the HF calorimeters, jets will activate both the electromagnetic (long fiber) and hadronic (short fiber) channels and a typical jet will occupy several adjacent towers. An afterpulse signal in one of these PMTs cannot be discriminated against (either in the trigger or in subsequent data analyses) and therefore will contribute to the total missing transverse energy in the event (see Figure 16). Also, we required presence of jet energy in a given tower 23, 24, and/or 25 crossings back (for type C PMTs) in order to take into account

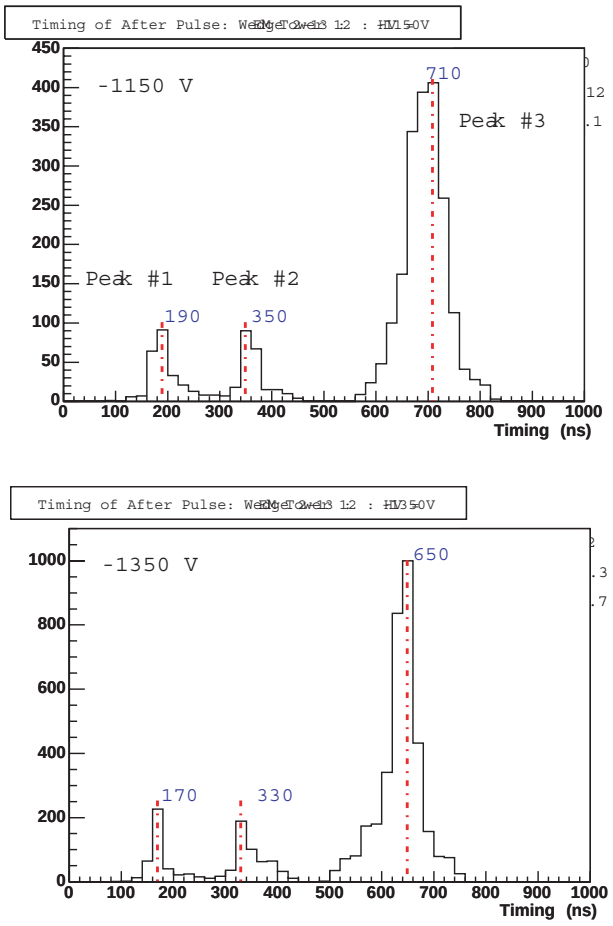

Figure 13: Reducing high voltage reduces the electric field between the photocathode and the first dynode. As a consequence, the afterpulse timing shifts by nearly 10% because drift time scales as $1/\sqrt{E}$.

a finite width of afterpulse arrival time.

We used PYTHIA to simulate the jet activity in the HF calorimeter. In each tower with a deposited energy larger than 20 GeV, we fired each channel at the rate consistent with what is shown in Figures 11 and with equivalent energy as in Figure 10. Therefore, we only summed the PMT afterpulse if it occurred in a channel that already had jet energy in it. This assumes that PMT afterpulses in isolated towers can be eliminated in subsequent analysis. This missing energy rate should be contrasted with a benchmark physics event at the LHC, $W \rightarrow l\nu$ decay rate for example. This suggests that the event rates from afterpulses only do not pose a significant background for missing E_t values of 20 GeV at these gain values. This background might be significant if the gain of the PMTs are increased by a factor of two, for example.

6 Conclusions

We draw the following conclusions from the results presented here:

1. The afterpulse rate depends on the amplitude of the main pulse (see Figures 11 and 14). For 100 GeV main pulse, we have a 1 to 10% chance of getting a 30 to 50 GeV afterpulse, depending on the PMT.

2. The afterpulse charge is approximately constant regardless of how it is generated (see Figures 10 and 15). Typically, the afterpulse equals 30 to 50 GeV at -1350V ($g \approx 10^5$).

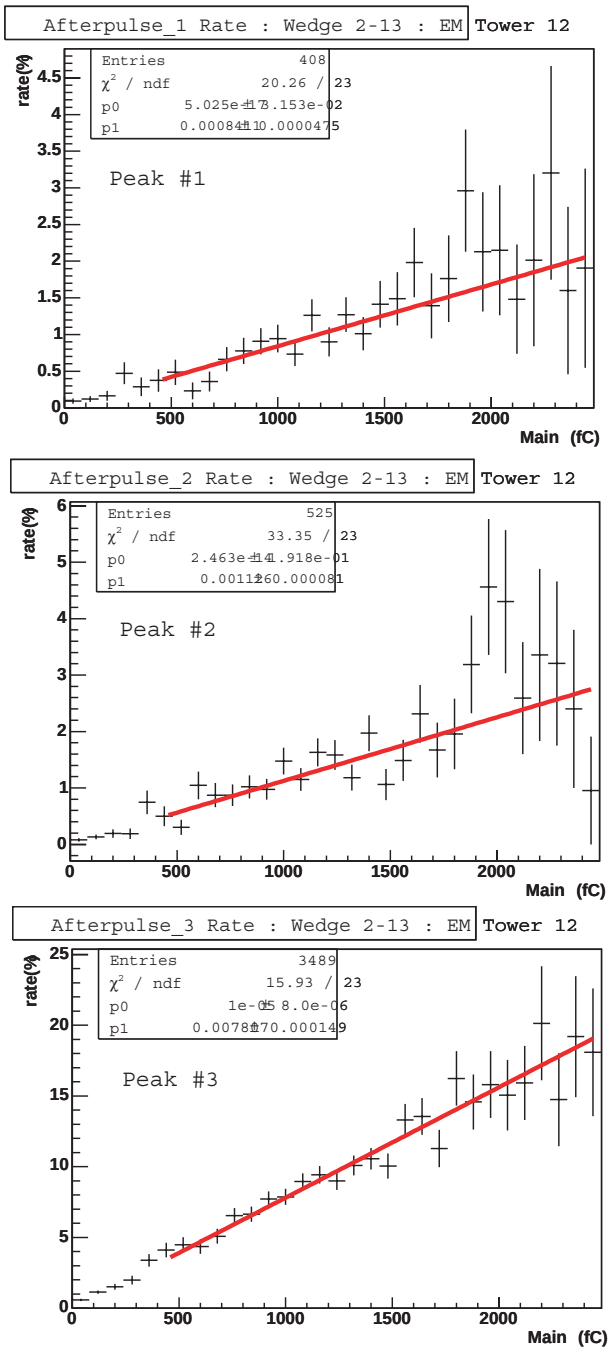

Figure 14: The rate of afterpulse for each of three peaks in time distribution is evaluated individually as a function of the main pulse charge. As the main pulse charge increases, the afterpulse rate increases linearly. The top, probably H_2^+ ion, shows an increase at the rate of 0.00084 %/fC. The other two peaks, probably He^2 and CH_4^+, show 0.0011 and 0.0078 %/fC rates, respectively.

3. The afterpulse rate does not depend on the hit rate up to 10^5 Hz as tested with LED pulses.

4. Although we did not show scope traces in this note, the afterpulses are very sharp, 3-10 ns in width.

5. There are three distinct types of gas contaminations in the PMT as seen in the time distributions. They come at 170, 330, and 650 ns later compared to the main pulse. We speculate that the first two come from hydrogen and helium and that the last one may come from methane, nitrogen, oxygen or a similarly heavy contaminant. At the present time, we do not have means of positively identifying these contaminants other than their flight times from the first dynode to the photocathode compared to electrons (in the opposite direction).

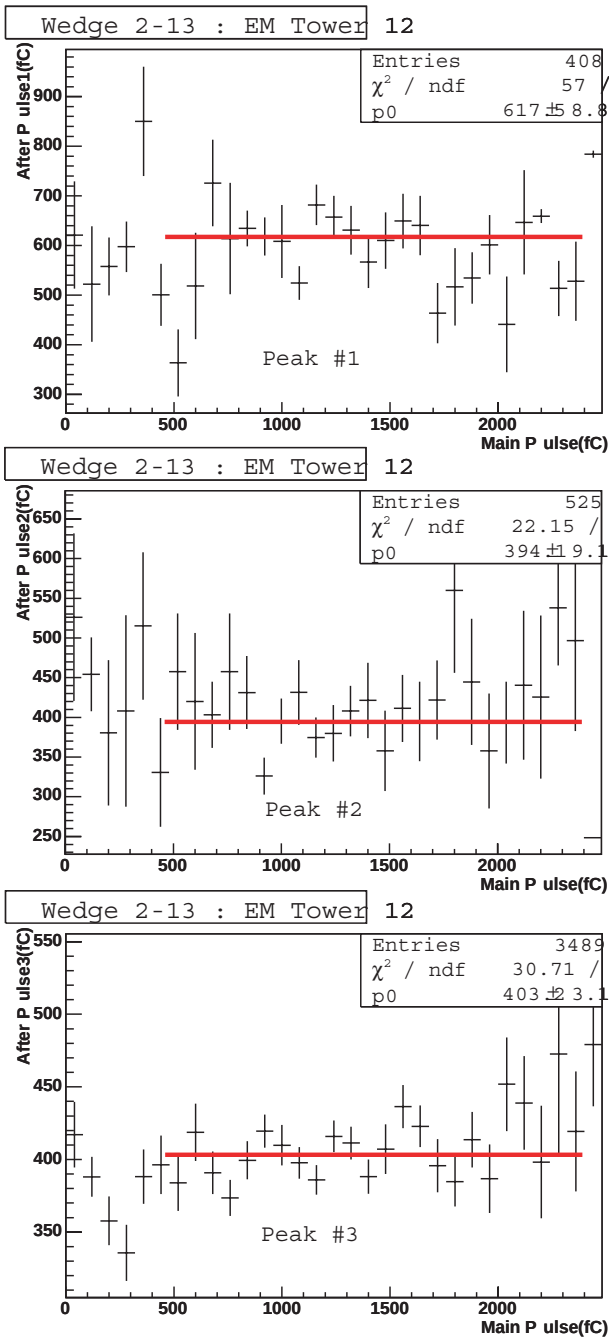

Figure 15: The afterpulse charge for each of the individual afterpulses identified in Figure 13 is nearly constant for each type between 35 to 55 GeV equivalent (11 fC/GeV).

6. The afterpulse rate will increase with increased gain of the PMT at a rate of $\sim 0.05\%$/V for a fixed PMT output signal, *i.e.* when the light level is adjusted such that the PMT output signal is the same as the HV is varied (see Figure 5).

7. The drift time of feed-back ions scales as $1/\sqrt{E}$ where E is the electric field between the photocathode and the first dynode (see Figure 13).

8. The total ionization cross section of 2×10^{-16} cm^2 for an 300 eV electron results in an ionization rate of 0.054 % for one electron at 1 ppm of partial pressure (or 0.067 %/GeV). This value is consistent with the measured value of 0.066 %/GeV if we assume 4 GeV per per single photoelectron and with a first dynode gain of 5.

9. The largest induced missing E_t generated by the afterpulses at the nominal PMT gain is around 20

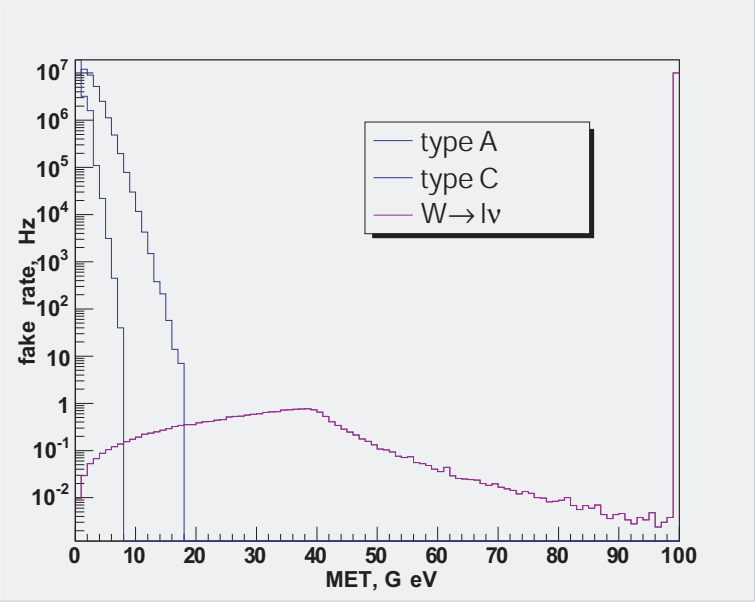

Figure 16: The transverse energy distribution due to afterpulses generated after 25 minimum bias events per beam crossing above the threshold of 20 GeV is calculated for type A and C PMTs (see Figure 14). The missing transverse energy distribution for $W \rightarrow l\nu$ decay is shown for comparison.

GeV at a rate of 20 Hz. Although missing transverse energy rate is high at low E_t values, this does not cause a serious problem. If, on the other hand, the PMT gain is increased by a factor of two or more, the afterpulse induced missing transverse energy rate will be comparable with W decay rate, for example.

7 Acknowledgement

The authors acknowledge fruitful discussions with J. Hauptman and E. Vlassov.

References

[1] http:jazz.uiowa.physics.edu

[2] R. Staubert *et al*, Nucl. Instr. Meth. **84** (1970) 297-300.

[3] S. S. Stevens and J. W. Longworth, IEEE Trans. NS-19(1) (1972) 356-359.

[4] G. A. Morton *et al*, IEEE Trans. NS-14(1) (1967) 443-448.

[5] G. P. Lamaze *et al* Nucl. Instr. Meth. **123** (1975) 403-404.

[6] S. J. Hall and J. McKeown, Nucl. Instr. Meth. **112** (1973) 545-549.

[7] V. Evdakimov and A. Evdakimov, D0 Note 4056, November 24, 2002.

[8] B. H. Candy, Rev. Sci. Instrum. **56** (2) (1985) 183-193.